Spectral selectivity in capillary dye lasers

ESMAEIL MOBINI[1,2], BEHNAM ABAIE[1,2], AND ARASH MAFI[1,2,*]

[1] Department of Physics & Astronomy, University of New Mexico, Albuquerque, NM 87131, USA
[2] Center for High Technology Materials, University of New Mexico, Albuquerque, NM 87106, USA
[*] Corresponding author: mafi@unm.edu

Compiled March 3, 2017

arXiv:1703.00620v1 [physics.optics] 2 Mar 2017

We explore the spectral properties of a capillary dye laser in the highly multimode regime. Our experiments indicate that the spectral behavior of the laser does not conform with a simple Fabry-Perot analysis; rather, it is strongly dictated by a Vernier resonant mechanism involving multiple modes, which propagate with different group velocities. The laser operates over a very broad spectral range and the Vernier effect gives rise to a free spectral range which is orders of magnitude larger than that expected from a simple Fabry-Perot mechanism. The presented theoretical calculations confirm the experimental results. Propagating modes of the capillary fiber are calculated using the finite element method (FEM) and it is shown that the optical path-lengths resulting from simultaneous beatings of these modes are in close agreement with the optical path-lengths directly extracted from the Fourier Transform of the experimentally measured laser emission spectra.

© 2017 Optical Society of America

OCIS codes: *(140.2050) Dye lasers; (060.3510) Lasers fiber; (140.3410) Laser resonators.*

http://dx.doi.org/10.1364/ao.XX.XXXXXX

Dye lasers have been a major player since mid 1960s with many attractive properties including a wide operating wavelength range, often spanning 50 to 100 nanometers, and can be reasonably efficient [1, 2]. However, because of the difficulties in handling the dyes which can be poisonous or even carcinogenic, and because of their rapid degradation during operation due to photo-bleaching, dye lasers have been mostly replaced with solid state lasers. Recent advances in optofluidic systems have brought attentions back to dye lasers again [3], primarily because dyes can be recirculated in such systems in enclosed set up mitigating the disadvantages while benefiting directly from their most favorable properties. Miniaturizing liquid dye lasers into a microfluidic device has many potential advantages such as compactness, easy maintenance, safe laser operation, accurate spatial mode control, and low threshold energy [3–7] with a wide range of applications including chemical and biological sensing [8, 9]. Microfluidic fiber lasers have also appeared in optical fiber platform resulting in dye fiber lasers [10–17]. Fiber lasers based on capillary tubes and photonic crystal fibers filled with a dye solution were studied in detail by Vasdekis et al. [10]. They reported a free spectral range (FSR) which was 300 times larger than what would be expected from a simple Fabry-Perot (FP) cavity analysis: they attributed this spectral selectivity to a Vernier resonant mechanism between two transversely propagating modes in the waveguide.

In this paper, we explore the operation of a dye-filled fiber laser in the highly multi-modal regime, giving rise to multiple peaks in the laser emission spectrum, with a considerably larger spectral range ($\sim$ 50 nm) compared with the two-mode operation regime reported by Vasdekis et al. We observe that a simple FP cavity analysis does not explain the FSR for the laser spectral modes, because it predicts spectral laser lines which are much more closely spaced than what we measure in the experiment. Here, we show that a Vernier resonant mechanism involving many operating modes is responsible for the observed large value of the FSR. We develop a theoretical model which accurately predicts the FSR based on the geometrical and optical properties of the fiber and its propagating spatial modes. The calculated spectral features show a good quantitative agreement with the experiment, confirming the important role of the Vernier resonant mechanism in setting the spectral behavior of similar fiber-based systems.

The fiber dye laser used here is a fused silica capillary of 5 µm inner, and 300 µm outer diameter, respectively. Rhodmaine 640 solution in benzyl alcohol at a concentration of 0.5 mg/ml was used to fill a few millimeter length of the fiber via capillary action. The benzyl alcohol solution and the cladding of the capillary have refractive indices of $n_{co} = 1.53$ and $n_{cl} = 1.46$, respectively. The relatively large refractive index contrast between fused silica cladding and benzyl solution in the fiber core enables the waveguide to operate in a highly multimodal regime. Calculations based on the V number of the capillary waveguide indicate that there are nearly 70 transverse modes guided by the capillary waveguide [18]. The gain medium is pumped through an SMF-28 optical fiber to maximize the pump intensity overlap with the gain volume. The optical pump source is a 0.6 ns pulsed frequency-doubled Nd:YAG laser at a repetition rate of 50 Hz. The output is collected by a 40X microscope objective and is sent into a spectrometer as shown in Fig. 1.

Figures. 2(a)-(d) show the emission spectra of the capillary dye laser for four different lengths of the capillary. Equation 1 is commonly used to calculated the FP cavity FSR; using this

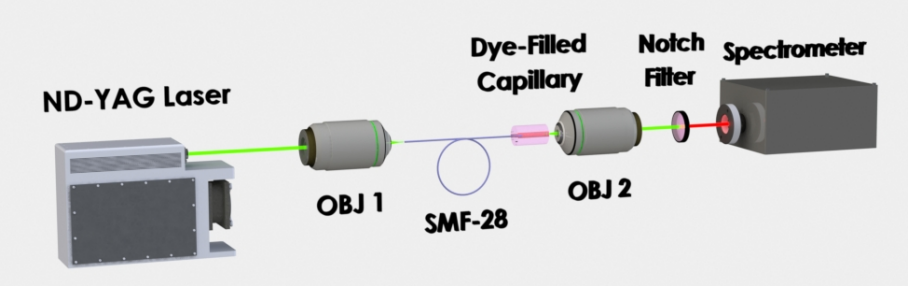

Fig. 1. A schematic of the experimental setup. Output of a pulse frequency doubled Nd:YAG laser is coupled into a single mode fiber. The single mode fiber is butt-coupled to the dye-filled capillary. The output is collected by a 40X microscope objective and sent into a spectrometer. Pump is filtered out using a notch filter.

equation for Fig. 2(d), e.g., gives

$$\Delta\lambda_{FSR} = \frac{\lambda^2}{2n_{co}L} \approx 0.014 \text{ nm}, \tag{1}$$

which is clearly much smaller than the FSR obsereved in Fig. 2(d).

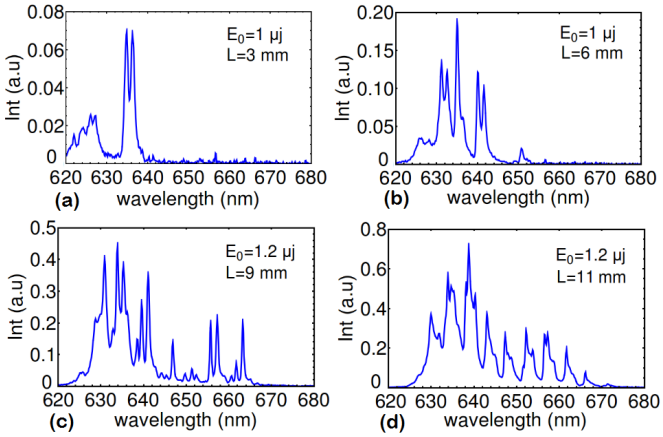

Fig. 2. (a) Emission spectra of the capillary dye laser with an input pulse energy of E_0 and length of (a) $L = 3$ mm, (b) $L = 6$ mm, (c) $L = 9$ mm, and (d) $L = 11$ mm.

In order to investigate the spectral behavior of the capillary laser, we assume that there are several propagating modes undergoing multiple round trips inside the capillary. The end reflections are due to the air-fiber/solvent interfaces at the capillary tips. Ignoring the polarization dynamics and assuming linearly polarized modes, we can expand the right-moving electric field propagating inside capillary as

$$E(\rho,\varphi,z) = E_0 \sum_{l=0}^{l_{max}} \sum_{m=1}^{m_{max}} A_{lm} J_l(\chi_{lm}\frac{\rho}{a}) e^{il\varphi} e^{i\beta_{lm}z}, \tag{2}$$

where β_{lm} are the propagation constants of the modes. J_l are Bessel functions of order l, which determine the transverse profile of the linearly polarized LP_{lm} modes. χ_{lm} is the m'th root of the J_l Bessel function. E_0 is an overall constant, A_{lm} is the complex amplitude coefficient of each mode, l ($l \in \{0, \sqrt{M}\}$) and m ($m \in \{1, \sqrt{M}-l)/2\}$) describe the azimuthal and radial distributions of the electric field components, respectively. $M \approx V^2/2$ is the total number of guided modes, $V = ka\sqrt{n_{co}^2 - n_{cl}^2}$ is the V parameter of the waveguide, $k = 2\pi/\lambda$, and a is the radius of the capillary core [18, 19].

The mode profiles and propagation constants can be numerically solved for using analytical expressions. In our analysis, we used a finite element method (FEM) code presented in Ref. [20] to calculate the propagation constants of the modes to a high accuracy.

Cavity loss from intrinsic attenuation and end mirrors are compensated by gain in the laser medium. Self-consistency requires the electric field of Eq. 2 to be reproduced after one round-trip. This translates into a series of conditions expressed as

$$e^{i\beta_{lm}2L} = 1, \quad \text{for all } l, m, \tag{3}$$

where L is the total length of the capillary. Of course, if a particular A_{lm} is equal to zero, i.e. that spatial mode is not excited because of symmetry or other reasons, then the corresponding phase condition in Eq. 3 does not need to be satisfied. Similarly, if the coefficient is small, i.e. the spatial mode carries a small power compared to other modes, the corresponding condition is less relevant and can likely be ignored. Here, we assume that the dominant mode which is excited in the capillary dye laser is the fundamental LP_{01} mode. Equation 3 can be expressed alternatively as

$$e^{i\beta_{01}2L} = 1, \tag{4a}$$

$$e^{i(\beta_{01}-\beta_{lm})2L} = 1, \quad \text{for all } l, m. \tag{4b}$$

The explicit separation of the phase term corresponding to LP_{01} mode makes it more convenient to apply the assumption that the LP_{01} mode is dominant in power. Equation 4a results in a standard FP form expressed in Eq. 1; however, because the resulting FSR in our configuration is considerably below our spectrometer resolution, this term does not have any effect on the shape of the measured spectrum and is averaged out as observed experimentally. Rather, it is Eq. 4b as the slow oscillating spectral term, which controls the location of the spectral features in our experiment.

In order to obtain the observed FSR from Eq. 4b, let us consider the case where the phase matching is satisfied at frequency ω_q, i.e. $[\beta_{01}(\omega_q) - \beta_{lm}(\omega_q)]2L = 2q\pi$, and q is an integer. The FSR is determined with $q+1$ at ω_{q+1}, where a Taylor expansion results in

$$\left(\partial\beta_{01}/\partial\omega - \partial\beta_{lm}/\partial\omega\right)\delta\omega = \pi/L. \tag{5}$$

This result can be cast in terms of the group indices of the modes

$$(n_{01}^{(g)} - n_{lm}^{(g)})\delta\omega = \frac{\pi c}{L} \rightarrow \delta\omega_{lm} = \frac{\pi c}{\Delta n^{(g)} L}, \tag{6}$$

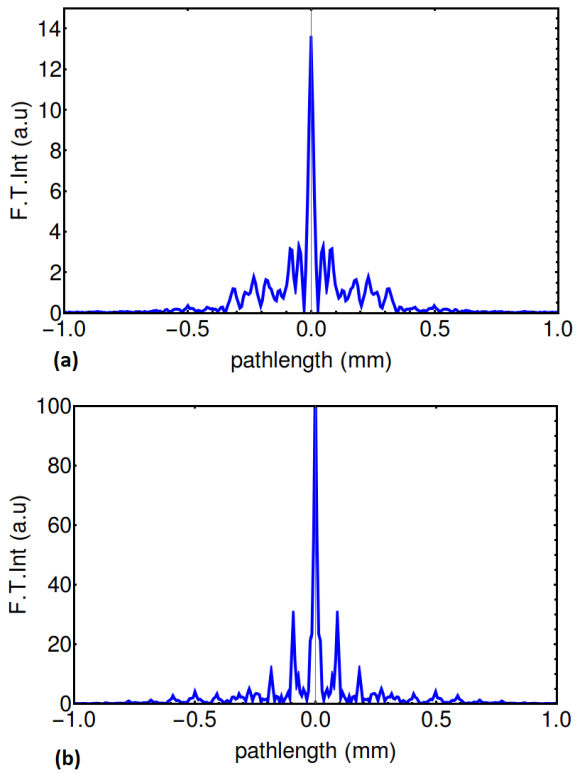

Fig. 3. (a) Fourier transform of the emission spectrum of the 6 mm capillary dye laser. (b) Fourier transform of the emission spectrum of the 11 mm capillary dye laser.

where $\Delta n^{(g)} = n_{01}^{(g)} - n_{lm}^{(g)}$.

In order to quantitatively investigate the validity of Eq. 6, we take the Fourier transform of the emission spectra of a 6 mm and an 11 mm capillary dye laser, as shown in Fig. 3 (a) and (b), respectively [10, 21–24]. The Fourier transform is performed in the space of the wave-vector k; therefore, the Fourier conjugate space is characterized by the optical pathlength d, whose peak positions d_{lm} relate to the spectral selectivity in Eq. 6 by

$$d_{lm} = 2L\Delta n_{lm}^{(g)} = \frac{2\pi c}{\delta\omega_{lm}}. \quad (7)$$

The peaks can be extracted from the Fourier transform data shown in Figs. 3(a) and (b). A simple comparison between Figs. 3(a) and (b) shows that the spacing between two neighboring peaks resulted from the 11 mm capillary is nearly two times larger than that resulted from the 6 mm capillary. This linear relationship is a strong indication of the longitudinal nature of the spectral selectivity mechanism in the capillary laser [10].

A more concrete proof can be obtained by directly calculating the values of d_{lm} using the fiber geometrical and optical parameters. Because we do not have access to the dispersion properties of the dye material, we make a reasonable assumption that the values of the group- and phase- velocity differences are nearly identical. We use the values of n_{co} and n_{cl} reported earlier and the core radius to calculate the propagation constants of the modes and establish the difference between the phase velocities of the fundamental mode and higher order modes. We note that by doing this, we are implicitly assuming that the majority of the laser power is concentrated in the fundamental mode because of the strong central pumping. It is possible to look at other mode combinations using the same formalism but we verified that our assumption captures the essence of the behavior of this capillary laser to a high degree of accuracy.

In Fig. 4, we show the values of d_{lm} directly calculated from the Fourier transform of the spectrum of the 11 mm capillary laser in Fig. 3 (b): the values of d_{lm} are extracted from the positions of the major peaks in the figure and shown as black circles in Fig. 4. Using the FEM code, we calculate $\Delta n^{(ph)} = n_{01}^{(ph)} - n_{lm}^{(ph)}$, which is the difference between the phase indices of the LP_{01} fundamental mode and the higher order modes. $\Delta n^{(ph)}$ is substituted in Eq. 7 in place of $\Delta n^{(g)}$, and the values of d_{lm} are shown as blue squares in Fig. 4. The strong quantitative resemblance between the experimental results and theoretical simulations indicate that our model is correct. Another way to see this result is directly in the frequency space, where e.g. the near periodic position of the peaks in Fig. 2 (d) with a peak-to-peak separation of around $\Delta\lambda \approx 5$ nm, is almost exactly as that calculated from the beating between LP_{01} and LP_{11} modes. This agrees well with a phase refractive index difference of $\Delta n_{11}^{(ph)} \approx 0.004$ calculated using the FEM code. Here, we take the wavelength associated with the maximum peak in Fig. 2 (d) which is around 640 nm to calculate the average FSR from Eq. 6.

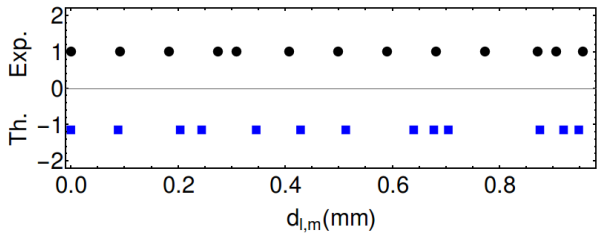

Fig. 4. The black column presents the extracted optical pathlengths from Fig. 3 (b). The blue column presents the resulted optical pathlengths from the calculated propagation constants inside the capillary.

Note that we only focused on the major peaks in Fig. 3 (b)– minor peaks are likely related to the beating among modes, not including the LP_{01} fundamental mode. The major sources of discrepancy are likely: 1) the substitution of $\Delta n^{(ph)}$ for $\Delta n^{(g)}$, and 2) the beating among higher order modes which are ignored in this analysis.

In conclusion, we have reported a detailed analysis of a capillary dye laser with a highly multimodal regime of operation. The intensity spectrum of the laser shows a FSR, which is much larger than what is expected from a naive FP analysis. It is shown that the spectral selectivity is dictated by a Vernier resonant mechanism, which is predominantly driven by the beating between the LP_{01} fundamental mode and higher order modes operating in the laser. The experimental values of the FSR have a strong quantitative resemblance to those calculated using the theoretical predictions.

REFERENCES

1. F. P. Schäfer, W. Schmidt, and J. Volze, "Organic dye solution laser," Applied Physics Letters **9** (1966).
2. F. Dörr, "F. p. schäfer (ed.): Topics in applied physics, vol. 1: Dye lasers, 2. revidierte auflage, springer-verlag, berlin, heidelberg, new york 1977. 298 s., 114 abb., preis: Dm 43,–," Berichte der Bunsengesellschaft für physikalische Chemie **82**, 670–670 (1978).

3. Z. Li and D. Psaltis, "Optofluidic dye lasers," Microfluidics and Nanofluidics **4**, 145–158 (2008).
4. B. Helbo, A. Kristensen, and A. Menon, "A micro-cavity fluidic dye laser," Journal of Micromechanics and Microengineering **13**, 307 (2003).
5. G. M. Whitesides, "The origins and the future of microfluidics," Nature **442**, 368–373 (2006).
6. T. Thorsen, S. J. Maerkl, and S. R. Quake, "Microfluidic large-scale integration," Science **298**, 580–584 (2002).
7. D. Psaltis, S. R. Quake, and C. Yang, "Developing optofluidic technology through the fusion of microfluidics and optics," Nature **442**, 381–386 (2006).
8. X. Fan and I. M. White, "Optofluidic microsystems for chemical and biological analysis," Nature photonics **5**, 591–597 (2011).
9. X. Fan and S.-H. Yun, "The potential of optofluidic biolasers," Nature methods **11**, 141–147 (2014).
10. A. E. Vasdekis, G. E. Town, G. A. Turnbull, and I. D. W. Samuel, "Fluidic fibre dye lasers," Opt. Express **15**, 3962–3967 (2007).
11. R. M. Gerosa, A. Sudirman, L. de S. Menezes, W. Margulis, and C. J. S. de Matos, "All-fiber high repetition rate microfluidic dye laser," Optica **2**, 186–193 (2015).
12. B. Abaie, E. Mobini, S. Karbasi, J. Ballato, and A. Mafi, "Observation of lasing in an anderson localizing optical fiber," in "CLEO: QELS_Fundamental Science," (Optical Society of America, 2016), pp. FM3D–4.
13. B. Abaie, E. Mobini, S. Karbasi, T. Hawkins, J. Ballato, and A. Mafi, "Random lasing in an anderson localizing optical fiber," arXiv preprint arXiv:1612.03835 (2016).
14. J.-H. Lin, Y.-L. Hsiao, B.-Y. Ciou, S.-H. Lin, Y.-H. Chen, and J.-J. Wu, "Manipulation of random lasing action from dye-doped liquid crystals infilling two-dimensional confinement single core capillary," IEEE Photonics Journal **7**, 1–9 (2015).
15. H. Zhou, G. Feng, K. Yao, C. Yang, J. Yi, and S. Zhou, "Fiber-based tunable microcavity fluidic dye laser," Optics letters **38**, 3604–3607 (2013).
16. A. Sudirman and W. Margulis, "All-fiber optofluidic component to combine light and fluid," Photonics Technology Letters, IEEE **26**, 1031–1033 (2014).
17. G. S. He, J. D. Bhawalkar, C. F. Zhao, C.-K. Park, and P. N. Prasad, "Two-photon-pumped cavity lasing in a dye-solution-filled hollow-fiber system," Optics letters **20**, 2393–2395 (1995).
18. B. E. A. Saleh and I. John Wiley & Sons, *Fundamentals of Photonics (Second Edition)* (Wiley-Interscience, 1991), 1st ed. Electronic reproduction. Somerset, New Jersey : Wiley InterScience, 2001. Available via World Wide Web.
19. K. Okamoto, *Fundamentals of Optical Waveguides*, Electronics & Electrical (Elsevier, 2006).
20. T. Lenahan, "Calculation of modes in an optical fiber using the finite element method and eispack," Bell System Technical Journal **62**, 2663–2694 (1983).
21. D. Hofstetter and R. L. Thornton, "Loss measurements on semiconductor lasers by fourier analysis of the emission spectra," Applied Physics Letters **72** (1998).
22. R. C. Polson, G. Levina, and Z. V. Vardeny, "Spectral analysis of polymer microring lasers," Applied Physics Letters **76** (2000).
23. A. Camposeo, M. Polo, P. Carro, L. Silvestri, S. Tavazzi, and D. Pisignano, "Random lasing in an organic light-emitting crystal and its interplay with vertical cavity feedback," Laser & Photonics Reviews **8**, 785–791 (2014).
24. A. J. Poustie, P. Harper, and N. Finlayson, "Multiwavelength fiber laser using a spatial mode beating filter," Optics letters **19**, 716–718 (1994).